5314 *Biochemistry* **2010,** *49,* 5314–5320
DOI: 10.1021/bi1007047

BIOCHEMISTRY
including biophysical chemistry & molecular biology
Article

Mechanism of the Calcium-Induced *trans*−*cis* Isomerization of a Non-Prolyl Peptide Bond in *Clostridium histolyticum* Collagenase[†]

Justin Spiriti[‡] and Arjan van der Vaart*[,§]

[‡]*Department of Chemistry and Biochemistry and Center for Biological Physics, Arizona State University, P.O. Box 871604, Tempe, Arizona 85287-1604, and* [§]*Department of Chemistry, University of South Florida, 4202 East Fowler Avenue, CHE 205, Tampa, Florida 33620*

Received May 5, 2010; Revised Manuscript Received May 24, 2010

ABSTRACT: *cis* peptide bonds in proteins are often rate-limiting steps in protein folding or conformational change and are frequently stabilized by metal ions. In the collagen-binding domain of *Clostridium histolyticum* collagenase, the binding of calcium ions triggers the formation of a *cis* peptide bond. We present free energy simulations of the formation of this *cis* peptide bond using a combined quantum mechanics/molecular mechanics approach together with adaptive umbrella sampling. From these simulations, we have determined that the calcium ions not only stabilize the *cis* peptide bond thermodynamically but also catalyze its formation; the free energy barrier to the formation of the *cis* peptide bond decreases from 21.4 kcal/mol in the absence of calcium ions to 10.3 kcal/mol in their presence. Two principal factors contribute to this reduction in the energy barrier. The calcium ions electrostatically stabilize the lone pair on the nitrogen atom that forms during the isomerization. In addition, their attraction to acidic amino acid side chains and formation of a hydrogen bond network constrain the peptide backbone in a way that makes it easier for the nitrogen to pyramidalize. Factors that explain the observed cooperativity of calcium binding are discussed.

Almost all peptide bonds in proteins are found to be in the *trans* conformation. This is especially true of peptide bonds that do not involve proline. In a survey of protein structures, 5.21% of peptide bonds to prolines and 0.029% of non-prolyl peptide bonds were found in the *cis* configuration (*1*). In another survey, merely 49 *cis* non-prolyl peptide bonds were found in a set of 747 protein structures (*2*). *cis* peptide bonds often have important functional or structural roles (*3*, *4*). For example, *cis*−*trans* isomerization acts as a conformational switch in signaling cascades (*4*−*6*) and is used as a timer for cellular processes (*7*).

Because of the partial double bond character of the peptide bond, *cis*−*trans* isomerization is characterized by a large energy barrier (*8*−*13*). Because of this barrier, *cis*−*trans* isomerization is often a rate-limiting step in protein folding (*14*, *15*). In vivo, the isomerization of proline-containing peptide bonds is accelerated by peptidyl prolyl *cis*−*trans* isomerases or rotamases (*2*, *16*, *17*). These ubiquitous enzymes are found in all cellular compartments and all organisms. While many prolyl isomerases have been identified, only one protein that accelerates the isomerization of non-prolyl peptide bonds has been found (*18*, *19*). In addition to its other functions as a chaperone (*20*, *21*), DnaK from *Escherichia coli* modestly enhances the isomerization of Ala−Xaa peptide bonds, where Xaa is Met, Ala, Ser, Glu, Leu, Ile, Gly, or Lys (*18*).

Apart from enzymes, certain metals like rhenium (*22*), cadmium (*23*, *24*), zinc (*24*), and lithium (*3*) have been shown to accelerate *cis*−*trans* isomerization and/or stabilize the *cis* conformer in peptide analogues. A survey of the Protein Data Bank showed that *cis* peptide bonds are frequently stabilized by calcium ions. For example, calcium binding induces a *trans*−*cis* prolyl peptide isomerization in bovine prothrombin (*25*), rat liver mannose binding protein (*26*), and the C-terminal domain of human BM-40 (*27*). In addition, calcium induces a *trans*−*cis* isomerization of a non-prolyl peptide bond in concanavalin A (*28*) and the collagen-binding domain of *Clostridium histolyticum* collagenase I (*29*). It is unclear how calcium stabilizes the *cis* states, and if and how calcium catalyzes the isomerization. For example, kinetic studies of rat liver mannose binding protein (*26*) showed no effect of calcium on the rate of isomerization, but the replacement of calcium with manganese ions significantly decelerated the *cis*−*trans* isomerization of concanavalin A (*30*). Molecular dynamics studies of the *cis* and *trans* prolyl peptide bond states in calcium-bound bovine prothrombin (*31*, *32*) showed little structural difference between the *cis* and *trans* protein; since only the end states of the isomerization and no free energies were calculated, the role of calcium for the *trans*−*cis* isomerization in bovine prothrombin remained unclear.

To investigate the role of calcium in the *cis*−*trans* isomerization of a peptide bond, we performed combined quantum mechanical/molecular mechanical free energy simulations of the collagen-binding domain (CBD)[1] of *C. histolyticum* collagenase class I. *C. histolyticum* is a Gram-positive bacterium, which causes gas gangrene (*33*). It produces two types of collagenases, which hydrolyze insoluble collagen fibrils, resulting in the extensive tissue destruction associated with the disease (*33*). Collagenase class I contains two CBDs, while collagenase class II has one; the three CBDs are homologous to each other (*34*−*37*).

[†]This work was supported by National Science Foundation CAREER Award CHE-1007816.

*To whom correspondence should be addressed. E-mail: avandervaart@usf.edu. Phone: (813) 974-8762. Fax: (813) 974-3203.

[1]Abbreviations: QM, quantum mechanics; MM, molecular mechanics; DFT, density functional theory; SCCDFTB, self-consistent charge density functional tight binding; CBD, collagen-binding domain; NMR, nuclear magnetic resonance.

 Published on Web 05/26/2010

The CBD of collagenase class I has been extensively studied by X-ray and NMR (*29*, *38*, *39*). Binding of calcium increases the affinity of the collagen-binding domain for collagen (*40*) and induces large conformational changes in the CBD, by refolding the N-terminal α-helical linker into a β-sheet (*29*). In collagenase I, the linker connects the CBDs; it is thought that the β-sheet rigidifies the protein, which increases the affinity for collagen (*29*, *41*).

In addition to the refolding, calcium binding also induces a non-prolyl *cis* peptide bond between E901 and N902. Since no enzyme is known to accelerate the isomerization of a Glu−Asn peptide bond, we decided to study this intriguing isomerization. Because the calcium binding pocket does not exist in the α-helical state, and since the barriers for refolding of the small linker are estimated to be much smaller than the barriers for isomerization, it is likely that refolding occurs before isomerization. Therefore, we focused on the isomerization reaction in the β-sheet conformation and will study the coupled refolding−isomerization transition in future work.

Our simulations show that calcium significantly decreases the free energy barrier for the *trans*−*cis* isomerization. While CBD binds two calcium ions, our results indicate that most of the reduction is obtained by the binding of the first calcium ion. Our structural analyses of the transition and end states explain how calcium stabilizes both the *cis* and transition states.

MATERIALS AND METHODS

The initial structure of the holoprotein was obtained from the Protein Data Bank [entry 1NQD (*29*)]. There are two calcium ions bound in the holo form, and the binding site involves the carboxyl groups of E899, E901, D904, D927, and D930, together with the backbone carbonyl groups of S922 and R929, the side chain amide oxygen of N903, and a crystallographic water molecule. The two binding sites are designated Ca1 and Ca2, with Ca2 being the binding site that is closer to the carbonyl oxygen of S902 and the carboxyl group of E899. A total of four systems were studied: the holoprotein with both calcium ions, the apoprotein with both calcium ions removed, and systems with one calcium bound in either the Ca1 or Ca2 pocket. The initial conformations of these systems were built from the holoprotein.

To better model the differences in energies and dipole moments between the *cis* and *trans* isomers, we treated the area around the E901−N902 peptide bond consisting of residues E901 and N902 and parts of K900 and N903 by quantum mechanics (QM). We used the SCCDFTB method (*42*, *43*) with a hydrogen bonding enhancement (*44*) for the QM calculations, because this method showed good agreement with higher-level methods and experiments for the *cis*−*trans* isomerization of cyclophilin A (*45*). To further test the quality of the SCCDFTB quantum mechanical method for our system, a Glu-Asn dipeptide was constructed and optimized in both *cis* and *trans* states at the B3LYP/6-31+g(d,p) and SCCDFTB levels. The peptide was blocked with an acetylated N-terminus, a C-terminal *N*-methylamide, and the Glu side chain was ionized. We used an ultrafine grid for the numerical integration of the exchange-correlation functional using the Gaussian software package (*46*).

While the area around the E901−N902 peptide bond was treated by QM, the rest of the system was treated by molecular mechanics (MM) (Figure 1). We used the CHARMM 22 force field (*47*) and CMAP enhancement (*48*) for the MM region, while covalent bonds between the QM and MM region were treated by the generalized hybrid orbital method (*49*, *50*). The protein was

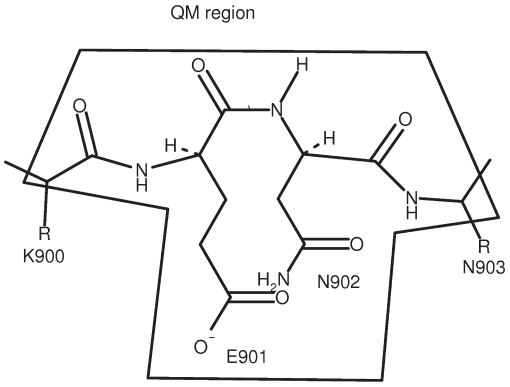

FIGURE 1: QM region used in this simulation.

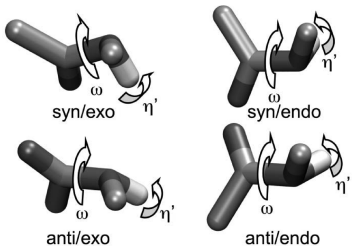

FIGURE 2: Definition of the ω and η' angles. ω is given by the dihedral angle involving E901 Cα, E901 C, N902 N, and N902 Cα; η is given by the improper dihedral angle involving E901 C, N902 Cα, N902 N, and N902 HN. η' has the same sign as η and is related to η by the equation $|\eta'| = 180 - |\eta'|$.

surrounded by explicit water (*51*) in a 61 Å × 65 Å × 53 Å box with a chloride ion for neutrality and periodic boundary conditions and the particle mesh Ewald method (*52*) in effect. A separate Ewald method was used to handle the QM/MM electrostatic interactions; for this, the κ value was set to 0.34 and **k** vectors with up to 6 components and magnitudes of up to 700 were used. A switching function between 8 and 12 Å was used for the van der Waals interactions. After minimization, the water was equilibrated while the protein was kept fixed. Calcium ions were then deleted for the apo and single-calcium simulations, with sodium ions added as necessary to achieve neutrality. After minimization, each system was heated to 300 K over 150 ps in the NPT ensemble with harmonic constraints on the MM protein backbone of 1.0 kcal mol^{-1} Å^{-1}. Once each system reached 300 K, the harmonic constraints were gradually removed in five steps over 50 ps, and the system was equilibrated in the NVT ensemble for an additional 50 ps. A constant temperature was maintained with the Berendsen thermostat (*53*), and all simulations were performed with CHARMM (*54*).

For each system, the relative free energies and barriers for the *cis*−*trans* interconversion of the E901−N902 peptide bond were determined by two-dimensional adaptive umbrella sampling simulations (*55*) using the ω and η' angles as coordinates (Figure 2). The ω reaction coordinate indicates the degree of peptide bond torsion, while the η' reaction coordinate indicates the degree of peptide nitrogen pyramidalization (*13*); these angles have been shown to be good reaction coordinates for peptide *cis*−*trans* isomerizations (*13*). The umbrella potential was readjusted every 100 ps using the negative of the potential of mean force calculated from all histograms from all runs using the weighted histogram analysis method (*56*). The umbrella biasing potential was expanded in an eighth-order trigonometric potential,

Table 1: Comparison of Charge Distributions and Isomerization Energies of a Capped Glu-Asn Dipeptide Calculated Using CHARMM, SCCDFTB, and DFT

quantity	B3LYP *cis*	SCCDFTB *cis*	CHARMM *cis*	B3LYP *trans*	SCCDFTB *trans*	CHARMM *trans*
dipole moment of peptide bond (D)	3.47	2.17	1.61	5.39	4.54	4.21
Mulliken charge for peptide C	0.19	0.48	0.51	0.33	0.47	0.51
Mulliken charge for peptide O	−0.49	−0.52	−0.51	−0.50	−0.56	−0.51
Mulliken charge for peptide N	−0.20	−0.30	−0.47	−0.13	−0.26	−0.47
Mulliken charge for peptide H	0.33	0.20	0.31	0.34	0.23	0.31
ΔE(*trans* → *cis*) (kcal/mol)	8.68	8.23	15.69			

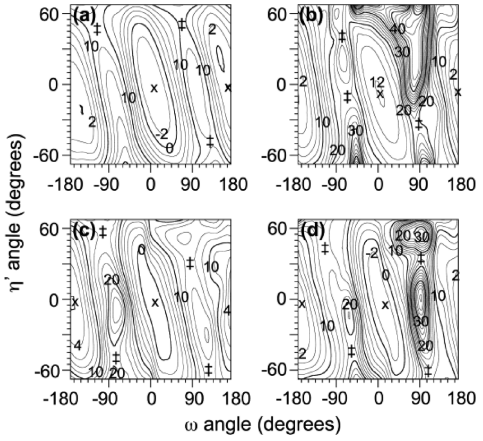

FIGURE 3: Two-dimensional contour plots of the potential of mean force as a function of ω and η' for the four binding states: (a) with both calcium ions, (b) without calcium ions, (c) with Ca1 only, and (d) with Ca2 only. Free energies shown are relative to the *trans* state of each peptide bond.

and the bin size of the histograms was 15°. Simulations were deemed converged when the maximum unsigned deviations between the binned free energies of the last two runs were within 0.40 kcal/mol, resulting in QM/MM adaptive umbrella sampling runs with 50−100 iterations, or a total duration between 5 and 10 ns. The locations of the transition states were identified as the lowest-energy saddle points on the final potential of mean force maps. To characterize each transition state structurally, we isolated the frames in each trajectory which had ω and η' values within 20° of the transition state for a separate examination. Each of these frames was analyzed for hydrogen bonds using a distance cutoff of 3.0 Å and an angle cutoff of 20°.

RESULTS

A comparison of the dipole moments and isomerization energies of the blocked Glu-Asn peptide showed a large improvement in SCCDFTB over the purely classical CHARMM potential (Table 1). The dipole moments of the *cis* and *trans* states are more enhanced in SCCDFTB and closer to the B3LYP values. Most notable is the drastic improvement of the isomerization energy, reducing the energy difference with B3LYP from 7.0 kcal/mol when using CHARMM to 0.4 kcal/mol when using SCCDFTB.

We used free energy QM/MM simulations at the SCCDFTB level to study the isomerization in the protein. Figure 3 shows the potentials of mean force for the *cis*−*trans* isomerization of the E901−N902 peptide bond as a function of the ω and η' angles (defined in Figure 1), and Table 2 lists the free energies of isomerization. By using a thermodynamic cycle involving calcium binding in the *cis* and *trans* states, as well as interconversion between these states, we also obtained the difference in binding free energies of calcium ions between the *cis* and *trans* states (Table 2). When both calcium ions were removed, the *trans* state of the peptide bond was much more thermodynamically stable than the *cis* state, consistent with the crystallographic finding that the *cis* peptide bond occurs only in the holoprotein (*29*). The presence of at least one calcium ion in the binding site caused the *cis* state to become more thermodynamically stable, however.

During the isomerization of an amide, the π bond between nitrogen and carbon is disrupted; as a consequence, the nitrogen becomes sp^3 hybridized with a pyramidal geometry, and there are in principle four possible transition states (*13*). Most of the possible transition states of the *cis*−*trans* isomerization could be identified as saddle points in the potentials of mean force. Their locations and heights are listed in Table 3. The presence of calcium ions significantly reduced the activation energy for

Table 2: Isomerization and Binding Free Energies of the Four QM/MM Simulations Performed in This Study[a]

simulation	ΔG(*trans* → *cis*) (kcal/mol)	$\Delta\Delta G_{bind}$ (kcal/mol)	convergence (kcal/mol)
both calcium ions	−3.8	−15.7	0.01
no calcium ions	11.9	0.0	0.40
Ca1 only	−1.6	−13.5	0.24
Ca2 only	−3.4	−15.3	0.01

[a] $\Delta\Delta G_{bind}$ values are relative to the state without calcium ions. Convergence refers to the maximum absolute deviation between free energies calculated on the last two runs.

Table 3: Approximate Locations and Heights of Free Energy Barriers Relative to the *trans* State for All Transition States Identified[a]

simulation	transition state	(ω,η')	$\Delta G^{\ddagger}$
both calcium ions	anti/endo	(−117°,49°)	11.2
	anti/exo	not observed	N/A
	syn/endo	**(68°,50°)**	**10.3**
	syn/exo	(129°,−49°)	11.8
no calcium ions	anti/endo	(−80°,45°)	24.5
	anti/exo	(−68°,−8°)	22.5
	syn/endo	not observed	N/A
	syn/exo	**(81°,−35°)**	**21.4**
Ca1 only	**anti/endo**	**(−99°,55°)**	**14.4**
	anti/exo	(−78°,−46°)	19.8
	syn/endo	(85°,33°)	14.5
	syn/exo	(125°,−63°)	15.1
Ca2 only	anti/endo	(−117°,46°)	15.2
	anti/exo	(−57°,−40°)	18.6
	syn/endo	(94°,36°)	17.9
	syn/exo	**(109°,−67°)**	**13.1**

[a] The lowest-energy transition state for each simulation is highlighted in bold.

Table 4: Averages and Standard Deviations of Mulliken Charges on Several Atoms of the QM Region in the Transition State

simulation	no. of frames	charge on peptide nitrogen	charge on E901 CD	charge on E901 OE1	charge on E901 OE2
both calcium ions	143	−0.40 ± 0.02	0.71 ± 0.02	−0.78 ± 0.05	−0.93 ± 0.05
no calcium ions	77	−0.38 ± 0.06	0.68 ± 0.02	−0.81 ± 0.04	−0.80 ± 0.04
Ca1 only	177	−0.40 ± 0.03	0.66 ± 0.02	−0.77 ± 0.04	−0.89 ± 0.03
Ca2 only	102	−0.41 ± 0.02	0.73 ± 0.02	−0.88 ± 0.05	−0.78 ± 0.06

Table 5: Manner in Which Calcium Ions Are Bound in the Different Simulations[a]

amino acid	both calcium ions	Ca1 only	Ca2 only
E899	binds Ca2 with two		binds Ca2 with two
E901	binds Ca1 and Ca2 with two	binds Ca1 with two	binds Ca2 with one
N903	binds Ca1	binds Ca1	
D904	binds Ca1 with one	binds Ca1 with one	
S922	binds Ca2		binds Ca2
D927	binds Ca1 and Ca2 with two	binds Ca1 with one	binds Ca2 with one
R929	binds Ca1		
D930	binds Ca2 with two	alternates between binding with one and binding with two	binds Ca2 with two

[a]Two refers to both carboxylate atoms, and one refers to one of the carboxylate atoms.

the formation of the *cis* peptide bond and also stabilized the *cis* state. When both calcium ions were bound in the active site, the barrier decreased to 10.3 kcal/mol. When only one calcium ion was present, the barrier assumed an intermediate value of 13−14 kcal/mol.

In addition to lowering the barrier, calcium also changed the mechanism of isomerization. Without calcium ions, the transition state peptide was in the exo configuration. When only Ca2 was present, the transition state was also in the exo configuration, but when Ca1 was present (either by itself or with Ca2), the transition state peptide nitrogen configuration changed from the exo to the endo configuration. The position of the lone pair in the transition state was affected by the electrostatic attraction of the calcium ions as well as repulsion by the carbonyl oxygen of K900. When only one calcium ion was present, the lone pair was on the side of the nitrogen closer to the calcium ions. When both calcium ions were present, the carbonyl oxygen of K900 occupied this space, forcing the lone pair to the opposite side of the nitrogen atom. Consequently, the change in mechanism from exo to endo was due to a combination of attraction of the lone pair on the peptide nitrogen to the calcium ions and its repulsion by the carbonyl oxygen of K900. Because of the attraction of this lone pair by the calcium ions, the Mulliken charge on the nitrogen atom in the transition state became more negative when either calcium ion was bound (Table 4). Only Ca2 was able to increase the polarization of the carboxyl group on E901. Therefore, the ability of Ca1 to polarize the peptide bond must be due to attraction to the electron density on the peptide nitrogen through space, rather than to a transfer of electron density through bonds from the peptide nitrogen to the carboxyl group.

When only one of the two calcium ions was present, the structure of the binding site changed to reflect this. These changes are summarized in Table 5. When only one ion was present, many of the acidic amino acids switch to binding the calcium ions with only one carboxylate oxygen atom, and as a result, their interactions with the calcium ions were weakened. These observations suggest that the calcium ions play important energetic and structural roles. They electrostatically stabilize the amino acids around them, forcing them into positions that maximize their interactions with the calcium ions, while at the same time restraining the position of the peptide backbone near the *cis* peptide bond. The side chain conformation of Glu901 in the transition state reflects this coupling among backbone, side chain, and calcium ions' electrostatic effects (Table 6). The (χ_1,χ_2) angle switched from the (gauche$^-$,anti) apo state to the (anti,gauche$^+$) fully bound state; for the singly bound Ca1 and Ca2 ions, the angles were (gauche$^-$,gauche$^-$) and (gauche$^-$,anti), respectively. Such correlations between the side chain and backbone conformation have been found in other systems as well (*57*−*61*).

The calcium-induced rearrangement of residues has large effects on the number and identity of hydrogen bonds in the binding site in the transition state (Table 6 and Figure 4). An analysis of these hydrogen bonding patterns suggests that the hydrogen bonds play a key role in stabilizing the transition state. The hydrogen bonds (in particular the one between E899 and N903) stabilized several amino acids that were near in sequence to the E901−N902 peptide bond, such as E899, N903, and D904. When Ca2 was present, the hydrogen bond between E899 and N903, together with the attraction between the side chains of E899, E901, and N903 and Ca2, forces the carbonyl carbon of E901 and the α-carbon of N903 closer together, helping the peptide nitrogen of N902 to pyramidalize. As a result, the transition state angle around the peptide nitrogen of N902 comes closer to the ideal value of 109.5° for an sp^3 hybridized atom when Ca2 is present. In addition, the peptide backbone conformation fluctuates less in this region in the transition state, as indicated by the lower values for the root-mean-square fluctuation (rmsf) for α-carbons shown in Figure 5.

Several other factors may contribute to the stabilization of the calcium ion binding site. Ca2 can also polarize the carboxyl group on E901, strengthening the electrostatic attraction, and while this study could not examine polarization in the other carboxyl groups, it is likely that they can be polarized similarly by the calcium ions. The presence of one calcium ion in the binding site also positioned and organized several amino acids around it, including those involved in binding both calcium ions. This reduces the entropic cost of binding the other calcium ion, which may explain the experimentally observed mild cooperativity in calcium binding (*41*).

The crystal structure of the apo form of the collagen-binding domain was found to have a larger hydrodynamic radius (*29*) and contain more and larger cavities than the holo form. This might be due to the electrostatic repulsion of the many carboxylates in the binding site, although part of the repulsion is relieved through conformational reorganization. For example, the side chains of E901 and D904 point toward the solvent in the apo state, and E899 forms a salt bridge with K900. The increase in the number

Table 6: Structural Characteristics of the Transition States[a]

simulation	no. of frames	important hydrogen bonds	E901 C−N902 N−N902 CA peptide bond angle (deg)	E901 CA−N902 CA distance (Å)	E901 C−N902 CA distance (Å)	E901 χ_1	E901 χ_2
both calcium ions	143	T910 OG1−N903 NH2 T910 OG1−K900 HN E899 COO−N903 NH2 E899 COO−S922 HN N902 OD1−D904 HN D930 COO−Y1002 OH Y1002 OH−Y932 OH	117.7 ± 3.9	3.2 ± 0.1	2.5 ± 0.1	anti	gauche$^+$
no calcium ions	77	D930 COO−N903 NH2 N903 O−Y931 HN Y931 O−T910 HN E899 COO−E899 HN	122.4 ± 4.4	3.4 ± 0.1	2.5 ± 0.1	gauche$^-$	anti
Ca1 only	177	N903 O−Y931 HN D904 COO−N903 HN Y931 O−T910 HN E899 COO−E899 HN Y932 OH−Y1002 OH	122.1 ± 4.4	3.6 ± 0.1	2.6 ± 0.1	gauche$^-$	gauche$^-$
Ca2 only	102	N903 OD1−T910 HG1 N903 OD1−T910 HN Y931 O−T910 HG1 K900 O−N903 NH2 E899 COO−N903 NH2 E899 COO−S922 HN Y1002 OH−Y932 OH	115.3 ± 3.9	3.6 ± 0.1	2.5 ± 0.1	gauche$^-$	anti

[a]Important hydrogen bonds and averages and standard deviations of angles and distances involving the peptide nitrogen and conformations of the E901 side chain in the transition state.

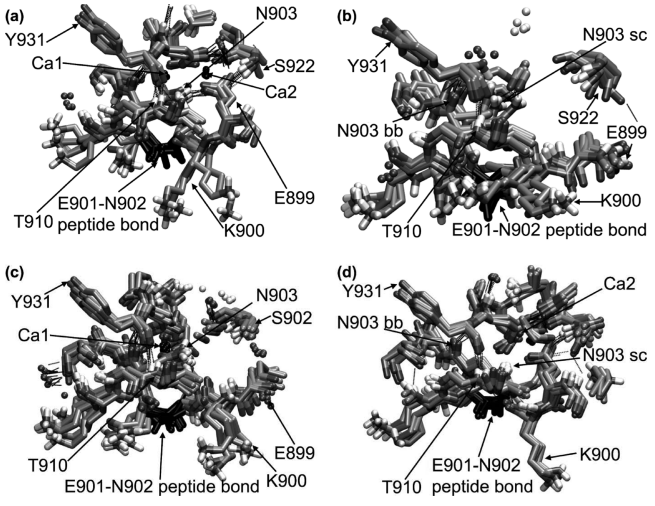

FIGURE 4: Transition states from the four simulations with important hydrogen bonds illustrated. The *cis* peptide bond is colored black: (a) with both calcium ions, (b) without calcium ions, (c) with Ca1 only, and (d) with Ca2 only.

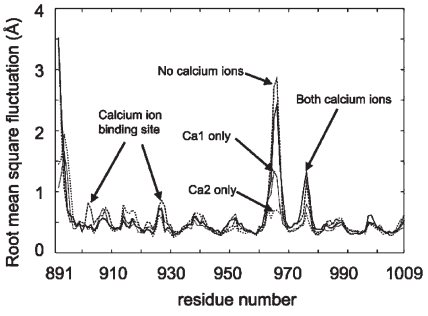

FIGURE 5: Root-mean-square fluctuation of α-carbons in the transition states.

and size of cavities is thought to destabilize the apo form of the protein compared to the holo form (*41*). Consequently, the ability of calcium ions to affect the number and size of cavities was examined. Measurements of the radii of gyration and measurements of the cavities of the protein (Table 7) indicate that the protein is less well packed when only one calcium ion was present than when no calcium ions or both calcium ions were present. In particular, when only one calcium ion is present, there was often a large pocket corresponding to the binding site of the other calcium ion, which may be maintained through electrostatic repulsion of the carboxylate groups not bound to calcium. The presence of this preformed binding site for the absent calcium ion provides a second explanation for the observed cooperativity of calcium binding (*41*).

DISCUSSION

While the particular calcium-binding motif in this protein is novel (*29*), there are many other known examples of proteins with two divalent ions coordinated close to one another. Although it does not have a *cis* peptide bond, the C_2 domain found in synaptotagmin and protein kinase C (*62*) shows many structural similarities to the collagen-binding domain considered here. Like the collagen-binding domain, the C_2 domain consists mostly of a *β*-barrel and also has a binding site that accommodates two calcium ions with coordination similar to that of the collagen-binding domain. Several other proteins are known to contain two magnesium ions coordinated to two aspartate residues, such as DNA polymerase (*63*, *64*) and fructose 1,6-bisphosphatase (*65*). In each case, the electrostatic repulsion between the two divalent ions is overcome by the negative charges that surround them. Similarly, in *C. histolyticum* collagenase, the two calcium ions are

Table 7: Averages and Standard Deviations of Radii of Gyration and Numbers, Total Surface Areas, and Total Volumes of Cavities for Each Simulation

simulation	radius of gyration (Å)	no. of cavities	total surface area of cavities (Å^2)	total volume of cavities (Å^3)
both calcium ions	13.75 ± 0.03	18.0 ± 3.2	793 ± 226	750 ± 263
no calcium ions	13.80 ± 0.06	17.7 ± 0.7	1062 ± 194	931 ± 315
Ca2 only	13.73 ± 0.03	23.4 ± 0.7	1111 ± 98	955 ± 133
Ca1 only	13.92 ± 0.09	20.8 ± 4.2	1294 ± 105	1188 ± 39

probably stabilized by the negative charges on all the residues surrounding them.

One of the potential functions of metal ions is stabilizing *cis* peptide bonds, such as those in bovine prothrombin (*25*), rat liver mannose binding protein (*26*), the C-terminal domain of human BM-40 (*27*), and concanavalin A (*28*). In *C. histolyticum* collagenase, we have established that the calcium ions reduce the activation barrier to the formation of the *cis* peptide bond between E901 and N902 in addition to stabilizing it thermodynamically, and we have examined some of the structural reasons for this.

The bound calcium ions catalyze the formation of the *cis* peptide bond through a combination of direct electrostatic effects on the atoms involved, as well as through their structural influence on the nearby peptide backbone. Each calcium ion performs a distinct role. Ca1 attracts this lone pair through space, changing the mechanism of isomerization. Ca2 stabilizes this lone pair by polarizing the bonds of E901 and also restrains E899 and E901 while forming hydrogen bonds involving the neighboring amino acids. This stabilizes the peptide backbone in a conformation in which it is easier for the peptide nitrogen of N902 to pyramidalize. Together, these effects result in a significant reduction in the free energy of activation of approximately 10 kcal/mol. The presence of one ion helps in the formation of the binding pocket for the second ion, which might explain the observed cooperativity of binding.

The observed stabilization of the ground and transition states might be important for other calcium-induced *trans*−*cis* isomerizations in proteins and may help explain the preference of calcium near *cis* peptide bonds.

ACKNOWLEDGMENT

We thank Dr. Hiqmet Kamberaj and Daniel Barr for discussions and Drs. Qiang Cui, Marcus Elstner, Prasad Phatak, and Jingzhi Pu for technical assistance with the SCCDFTB method. We thank the Arizona State University Fulton HPCI and the Teragrid for computer time.

REFERENCES

1. Jabs, A., Weiss, M. S., and Hilgenfeld, R. (1999) Non-proline cis peptide bonds in proteins. *J. Mol. Biol. 286*, 291–304.
2. Schmid, F. X. (2002) Prolyl isomerases. In Protein Folding in the Cell, pp 243−282, Academic Press Inc., San Diego.
3. Dugave, C., and Demange, L. (2003) Cis-trans isomerization of organic molecules and biomolecules: Implications and applications. *Chem. Rev. 103*, 2475–2532.
4. Andreotti, A. H. (2003) Native state proline isomerization: An intrinsic molecular switch. *Biochemistry 42*, 9515–9524.
5. Min, L., Fulton, D. B., and Andreotti, A. H. (2005) A case study of proline isomerization in cell signaling. *Front. Biosci. 10*, 385–397.
6. Isakov, N. (2008) A new twist to adaptor proteins contributes to regulation of lymphocyte cell signaling. *Trends Immunol. 29*, 388–396.
7. Lu, K. P., Finn, G., Lee, T. H., and Nicholson, L. K. (2007) Prolyl cis-trans isomerization as a molecular timer. *Nat. Chem. Biol. 3*, 619–629.
8. Gutierrez, L. J., Baldoni, H. A., and Enriz, R. D. (2009) Conformational and electronic study of cis-peptides (non-proline residues) occurring in natural proteins. *J. Mol. Struct. 934*, 103–111.
9. Jorgensen, W. L., and Gao, J. (1988) Cis trans energy difference for the peptide-bond in the gas-phase and in aqueous-solution. *J. Am. Chem. Soc. 110*, 4212–4216.
10. Mantz, Y. A., Branduardi, D., Bussi, G., and Parrinello, M. (2009) Ensemble of transition state structures for the cis-trans isomerization of N-methylacetamide. *J. Phys. Chem. B 113*, 12521–12529.
11. Schroeder, O. E., Carper, E., Wind, J. J., Poutsma, J. L., Etzkorn, F. A., and Poutsma, J. C. (2006) Theoretical and experimental investigation of the energetics of cis-trans proline isomerization in peptide models. *J. Phys. Chem. A 110*, 6522–6530.
12. Kang, Y. K., and Choi, H. Y. (2004) Cis-trans isomerization and puckering of proline residue. *Biophys. Chem. 111*, 135–142.
13. Fischer, S., Dunbrack, R. L., and Karplus, M. (1994) Cis-trans imide isomerization of the proline dipeptide. *J. Am. Chem. Soc. 116*, 11931–11937.
14. Wedemeyer, W. J., Welker, E., and Scheraga, H. A. (2002) Proline cis-trans isomerization and protein folding. *Biochemistry 41*, 14637–14644.
15. Odefry, C., Mayr, L. M., and Schmid, F. X. (1995) Non-prolyl cis-trans peptide bond isomerization as a rate-determining step in protein unfolding and refolding. *J. Mol. Biol. 245*, 69–78.
16. Fanghanel, J., and Fischer, G. (2004) Insights into the catalytic mechanism of peptidyl prolyl cis/trans isomerases. *Front. Biosci. 9*, 3453–3478.
17. Gothel, S. F., and Marahiel, M. A. (1999) Peptidyl-prolyl cis-trans isomerases, a superfamily of ubiquitous folding catalysts. *Cell. Mol. Life Sci. 55*, 423–436.
18. Schiene-Fischer, C., Habazettl, J., Schmid, F. X., and Fischer, G. (2002) The Hsp70 chaperone DnaK is a secondary amide peptide bond cis-trans isomerase. *Nat. Struct. Biol. 9*, 419–424.
19. Swain, J. F., and Gierasch, L. M. (2002) A new twist for an Hsp70 chaperone. *Nat. Struct. Biol. 9*, 406–408.
20. Genevaux, P., Georgopoulos, C., and Kelley, W. L. (2007) The Hsp70 chaperone machines of *Escherichia coli*: A paradigm for the repartition of chaperone functions. *Mol. Microbiol. 66*, 840–857.
21. Goloubinoff, P., and De Los Rios, P. (2007) The mechanism of Hsp70 chaperones: (entropic) Pulling the models together. *Trends Biochem. Sci. 32*, 372–380.
22. Meiere, S. H., Ding, F., Friedman, L. A., Sabat, M., and Harman, W. D. (2002) Dihapto coordination of carboxylic acid derivatives with an asymmetric rhenium π-base: A new mechanism for amide isomerization? *J. Am. Chem. Soc. 124*, 13506–13512.
23. Niklas, N., Hampel, F., Liehr, G., Zahl, A., and Alsfasser, R. (2001) The reactivity of N-coordinated amides in metallopeptide frameworks: Molecular events in metal-induced pathogenic pathways? *Chem.—Eur. J. 7*, 5135.
24. Niklas, N., Zahl, A., and Alsfasser, R. (2007) Transesterification and amide cis-trans isomerization in Zn and Cd complexes of the chelating amino acid ligand Boc-Asp(Dpa)-OBzl. *Dalton Trans.*, 154–162.
25. Evans, T. C., and Nelsestuen, G. L. (1996) Importance of cis-proline 22 in the membrane-binding conformation of bovine prothrombin. *Biochemistry 35*, 8210–8215.
26. Ng, K. K.-S., and Weis, W. I. (1998) Coupling of prolyl peptide bond isomerization and Ca^{2+} binding in a C-type mannose-binding protein. *Biochemistry 37*, 17977–17989.
27. Hohenester, E., Maurer, P., Hohenadl, C., Timpl, R., Jansonius, J. N., and Engel, J. (1996) Structure of a novel extracellular Ca^{2+}-binding module in BM-40. *Nat. Struct. Biol. 3*, 67–73.
28. Brewer, C. F., Brown, R. D., and Koenig, S. H. (1983) Metal-ion binding and conformational transitions in concanavalin-A: A structure-function study. *J. Biomol. Struct. Dyn. 1*, 961–997.
29. Wilson, J. J., Matsushita, O., Okabe, A., and Sakon, J. (2003) A bacterial collagen-binding domain with novel calcium-binding motif controls domain orientation. *EMBO J. 22*, 1743–1752.
30. Bouckaert, J., Dewallef, Y., Poortmans, F., Wyns, L., and Loris, R. (2000) The structural features of concanavalin A governing non-proline peptide isomerization. *J. Biol. Chem. 275*, 19778–19787.
31. Charifson, P. S., Darden, T., Tulinsky, A., Hughey, J. L., Hiskey, R. G., and Pedersen, L. G. (1991) Solution conformations of the

γ-carboxyglutamic acid domain of bovine prothrombin fragment-1, residues 1−65. *Proc. Natl. Acad. Sci. U.S.A. 88*, 424–428.
32. Perera, L., Darden, T. A., and Pederson, L. G. (1998) Trans-cis isomerization of proline 22 in bovine prothrombin fragment 1: A surprising result of structural characterization. *Biochemistry 37*, 10920–10927.
33. Harrington, D. J. (1996) Bacterial collagenases and collagen-degrading enzymes and their potential role in human disease. *Infect. Immun. 64*, 1885–1891.
34. Matsushita, O., Jung, C. M., Minami, J., Katayama, S., Nishi, N., and Okabe, A. (1998) A study of the collagen-binding domain of a 116-kDa *Clostridium histolyticum* collagenase. *J. Biol. Chem. 273*, 3643–3648.
35. Toyoshima, T., Matsushita, O., Minami, J., Nishi, N., Okabe, A., and Itano, T. (2001) Collagen-binding domain of a *Clostridium histolyticum* collagenase exhibits a broad substrate spectrum both in vitro and in vivo. *Connect. Tissue Res. 42*, 281.
36. Yoshihara, K., Matsushita, O., Minami, J., and Okabe, A. (1994) Cloning and nucleotide-sequence analysis of the ColH gene from *Clostridium histolyticum* encoding a collagenase and a gelatinase. *J. Bacteriol. 176*, 6489–6496.
37. Matsushita, O., Jung, C. M., Katayama, S., Minami, J., Takahashi, Y., and Okabe, A. (1999) Gene duplication and multiplicity of collagenases in *Clostridium histolyticum*. *J. Bacteriol. 181*, 923–933.
38. Philominathan, S. T. L., Matsushita, O., Jordan, J. B., and Sakon, J. (2008) H-1, C-13 and N-15 resonance assignments of Ca^{2+} bound collagen-binding domain derived from a clostridial collagenase. *Biomol. NMR Assignments 2*, 127–129.
39. Philominathan, S. T. L., Koide, T., Hamada, K., Yasui, H., Seifert, S., Matsushita, O., and Sakon, J. (2009) Unidirectional binding of clostridial collagenase to triple helical substrates. *J. Biol. Chem. 284*, 10868–10876.
40. Matsushita, O., Koide, T., Kobayahsi, R., Nakata, K., and Okabe, A. (2001) Substrate recognition by the collagen-binding domain of *Clostridium histolyticum* class I collagenase. *J. Biol. Chem. 276*, 8761–8770.
41. Philominathan, S. T. L., Matsushita, O., Gensure, R., and Sakon, J. (2009) Ca^{2+}-induced linker transformation leads to a compact and rigid collagen-binding domain of *Clostridium histolyticum* collagenase. *FEBS J. 276*, 3589–3601.
42. Elstner, M., Porezag, D., Jungnickel, G., Elsner, J., Haugk, M., Frauenheim, T., Suhai, S., and Seifert, G. (1998) Self-consistent charge density-functional tight-binding method for simulations of complex materials properties. *Phys. Rev. B 58*, 7260–7268.
43. Cui, Q., Elstner, M., Kaxiras, E., Frauenheim, T., and Karplus, M. (2001) A QM/MM implementation of the self-consistent charge density functional tight binding (SCC-DFTB) method. *J. Phys. Chem. B 105*, 569–585.
44. Yang, Y., Yu, H., York, D., Cui, Q., and Elstner, M. (2007) Extension of the self-consistent-charge density-functional tight-binding method: Third-order expansion of the density functional theory total energy and introduction of a modified effective Coulomb interaction. *J. Phys. Chem. A 111*, 10861–10873.
45. Li, G. H., and Cui, Q. (2003) What is so special about Arg 55 in the catalysis of cyclophilin A? Insights from hybrid QM/MM simulations. *J. Am. Chem. Soc. 125*, 15028–15038.
46. Frisch, M. J., Trucks, G. W., Schlegel, H. B., Scuseria, G. E., Robb, M. A., Cheeseman, J. R., Montgomery, J. A., Jr., Vreven, T., Kudin, K. N., Burant, J. C., Millam, J. M., Iyengar, S. S., Tomasi, J., Barone, V., Mennucci, B., Cossi, M., Scalmani, G., Rega, N., Petersson, G. A., Nakatsuji, H., Hada, M., Ehara, M., Toyota, K., Fukuda, R., Hasegawa, J., Ishida, M., Nakajima, T., Honda, Y., Kitao, O., Nakai, H., Klene, M., Li, X., Knox, J. E., Hratchian, H. P., Cross, J. B., Bakken, V., Adamo, C., Jaramillo, J., Gomperts, R., Stratmann, R. E., Yazyev, O., Austin, A. J., Cammi, R., Pomelli, C., Ochterski, J. W., Ayala, P. Y., Morokuma, K., Voth, G. A., Salvador, P., Dannenberg, J. J., Zakrzewski, V. G., Dapprich, S., Daniels, A. D., Strain, M. C., Farkas, O., Malick, D. K., Rabuck, A. D., Raghavachari, K., Foresman, J. B., Ortiz, J. V., Cui, Q., Baboul, A. G., Clifford, S., Cioslowski, J., Stefanov, B. B., Liu, G., Liashenko, A., Piskorz, P., Komaromi, I., Martin, R. L., Fox, D. J., Keith, T., Al-Laham, M. A., Peng, C. Y., Nanayakkara, A., Challacombe, M., Gill, P. M. W., Johnson, B., Chen, W., Wong, M. W., Gonzalez, C., and Pople, J. A. (2003) Gaussian 03, Gaussian, Inc., Wallingford, CT.
47. MacKerell, A. D., Jr., Bashford, D., Bellot, M., Dunbrack, R. L., Jr., Evanseck, J. D., Field, M. J., Fischer, S., Gao, J., Guo, H., Ha, S., Joseph-McCarthy, D., Kuchnir, L., Kuczera, K., Lau, F. T. K., Mattos, C., Michnick, S., Ngo, T., Nguyen, D. T., Prodhom, B., Reiher, W. E., III, Roux, B., Schlenkrich, M., Smith, J. C., Stote, R., Straub, J., Watanabe, M., Wiórkiewicz-Kuczera, J., Yin, D., and Karplus, M. (1998) All-atom empirical potential for molecular modeling and dynamics studies of proteins. *J. Phys. Chem. B 102*, 3586–3616.
48. MacKerell, A. D., Jr., Feig, M., and Brooks, C. L., III (2004) Extending the treatment of backbone energetics in protein force fields: Limitations of gas-phase quantum mechanics in reproducing protein conformational distributions in molecular dynamics simulations. *J. Comput. Chem. 25*, 1400–1415.
49. Gao, J., Amara, P., Alhambra, C., and Field, M. J. (1998) A generalized hybrid orbital (GHO) method for the treatment of boundary atoms in combined QM/MM calculations. *J. Phys. Chem. A 102*, 4714–4721.
50. Pu, J., Gao, J., and Truhler, D. G. (2004) Combining self-consistent charge density-functional tight-binding (SCC-DFTB) with molecular mechanics by the generalized hybrid orbital (GHO) method. *J. Phys. Chem. A 108*, 5454–5463.
51. Jorgensen, W., Chandrasekar, J., Madura, J., Impey, R., and Klein, M. (1983) Comparison of simple potential functions for simulating liquid water. *J. Chem. Phys. 79*, 926–935.
52. Essmann, U., Perera, L., Berkowitz, M., Darden, T., Lee, H., and Pedersen, L. G. (1995) A smooth particle mesh Ewald method. *J. Chem. Phys. 103*, 8577–8593.
53. Berendsen, H. J. C., Postma, J. P. M., van Gunsteren, W. F., DiNola, A., and Haak, J. R. (1984) Molecular dynamics with coupling to an external bath. *J. Chem. Phys. 81*, 3684–3690.
54. Brooks, B. R., Brooks, C. L., III, MacKerell, A. D., Jr., Nilsson, L., Petrella, R. J., Roux, B., Won, Y., Archontis, G., Bartels, C., Boresch, S., Caflisch, A., Caves, L., Cui, Q., Dinner, A. R., Feig, M., Fischer, S., Gao, J., Hodoscek, M., Im, W., Kuczera, K., Lazaridis, T., Ma, J., Ovchinnikov, V., Paci, E., Pastor, R. W., Post, C. B., Pu, J. Z., Schaefer, M., Tidor, B., Venable, R. M., Woodcock, H. L., Wu, X., Yang, W., York, D. M., and Karplus, M. (2009) CHARMM: The biomolecular simulation program. *J. Comput. Chem. 30*, 1545–1614.
55. Bartels, C., and Karplus, M. (1997) Multidimensional adaptive umbrella sampling: Applications to main chain and side chain peptide conformations. *J. Comput. Chem. 18*, 1450–1462.
56. Ferrenberg, A. M., and Swendsen, R. H. (1989) Optimized Monte-Carlo data-analysis. *Phys. Rev. Lett. 63*, 1195–1198.
57. Henchman, R. H., Kilburn, J. A., Turner, D. L., and Essex, J. W. (2004) Conformational and enantioselectivity in host-guest chemistry: The selective binding of cis amides examined by free energy calculations. *J. Phys. Chem. B 108*, 17571–17582.
58. Jiang, F., Han, W., and Wu, Y. D. (2010) Influence of Side Chain Conformations on Local Conformational Features of Amino Acids and Implication for Force Field Development. *J. Phys. Chem. B 114*, 5840–5850.
59. Dunbrack, R. L., and Karplus, M. (1993) Backbone-dependent rotamer library for proteins: Application to side-chain prediction. *J. Mol. Biol. 230*, 543–574.
60. Dunbrack, R. L., and Cohen, F. E. (1997) Bayesian statistical analysis of protein side-chain rotamer preferences. *Protein Sci. 6*, 1661–1681.
61. Dunbrack, R. L., and Karplus, M. (1994) Conformational-analysis of the backbone-dependent rotamer preferences of protein side-chains. *Nat. Struct. Biol. 1*, 334–340.
62. Shao, X. G., Davletov, B. A., Sutton, R. B., Sudhof, T. C., and Rizo, J. (1996) Bipartite Ca^{2+}-binding motif in C-2 domains of synaptotagmin and protein kinase C. *Science 273*, 248–251.
63. Davies, J. F., Almassy, R. J., Hostomska, Z., Ferre, R. A., and Hostomsky, Z. (1994) 2.3-Ångstrom crystal-structure of the catalytic domain of DNA polymerase-β. *Cell 76*, 1123–1133.
64. Pelletier, H., Sawaya, M. R., Kumar, A., Wilson, S. H., and Kraut, J. (1994) Structures of ternary complexes of rat DNA-polymerase-β, a DNA template-primer, and DDCTP. *Science 264*, 1891–1903.
65. Xue, Y. F., Huang, S. H., Liang, J. Y., Zhang, Y. P., and Lipscomb, W. N. (1994) Crystal-structure of fructose-1,6-bisphosphatase complexed with fructose 2,6-bisphosphate, AMP, and Zn^{2+} at 2.0-Ångstrom resolution: Aspects of synergism between inhibitors. *Proc. Natl. Acad. Sci. U.S.A. 91*, 12482–12486.